General Framework for Studying the Dynamics of Folded and Nonfolded Proteins by NMR Relaxation Spectroscopy and MD Simulation

ARTICLE *in* JOURNAL OF THE AMERICAN CHEMICAL SOCIETY · MAY 2002

Impact Factor: 12.11 · DOI: 10.1021/ja012750u · Source: PubMed

J|A|C|S
ARTICLES
Published on Web 03/30/2002

General Framework for Studying the Dynamics of Folded and Nonfolded Proteins by NMR Relaxation Spectroscopy and MD Simulation

Jeanine J. Prompers and Rafael Brüschweiler*

Contribution from the Carlson School of Chemistry and Biochemistry, Clark University, Worcester, Massachusetts 01610

Received December 21, 2001. Revised Manuscript Received February 7, 2002

Abstract: A general framework is presented for the interpretation of NMR relaxation data of proteins. The method, termed isotropic reorientational eigenmode dynamics (iRED), relies on a principal component analysis of the isotropically averaged covariance matrix of the lattice functions of the spin interactions responsible for spin relaxation. The covariance matrix, which is evaluated using a molecular dynamics (MD) simulation, is diagonalized yielding reorientational eigenmodes and amplitudes that reveal detailed information about correlated protein dynamics. The eigenvalue distribution allows one to quantitatively assess whether overall and internal motions are statistically separable. To each eigenmode belongs a correlation time that can be adjusted to optimally reproduce experimental relaxation parameters. A key feature of the method is that it does not require separability of overall tumbling and internal motions, which makes it applicable to a wide range of systems, such as folded, partially folded, and unfolded biomolecular systems and other macromolecules in solution. The approach was applied to NMR relaxation data of ubiquitin collected at multiple magnetic fields in the native form and in the partially folded A-state using MD trajectories with lengths of 6 and 70 ns. The relaxation data of native ubiquitin are well reproduced after adjustment of the correlation times of the 10 largest eigenmodes. For this state, a high degree of separability between internal and overall motions is present as is reflected in large amplitude and collectivity gaps between internal and overall reorientational modes. In contrast, no such separability exists for the A-state. Residual overall tumbling motion involving the N-terminal β-sheet and the central helix is observed for two of the largest modes only. By adjusting the correlation times of the 10 largest modes, a high degree of consistency between the experimental relaxation data and the iRED model is reached for this highly flexible biomolecule.

1. Introduction

NMR spin relaxation measurements offer important insights into protein mobility at atomic resolution.[1−6] The objective is to obtain information about motional amplitudes, collective dynamics, and correlation times and their dependence on different factors, such as temperature, buffer condition, the presence of ligands, and mutations. Such information can be further used to establish a connection between dynamics and entropy, which helps to unravel the driving forces behind protein function.[7]

Spin relaxation is manifested in NMR in the form of dissipative evolution of the spin-density operator $\sigma(t)$. The physical origin of spin relaxation is the stochastic modulation of nuclear spin interactions due to protein motion. The relevant statistical properties are the variances and covariances of the lattice functions of these interactions that can be compiled in a covariance matrix **M** together with a set of correlation times $\{\tau_m\}$.[8] The eigenvalues and eigenvectors of matrix **M** depict amplitudes and directions of the eigenmodes of protein dynamics containing information about motional correlation effects.

Scheme 1

covariance matrix $\boldsymbol{M}$, $\{\tau_m\}$ $\underset{\text{reconstruction}}{\overset{\text{spin relaxation}}{\rightleftharpoons}}$ density operator evolution $\sigma(t)$

A general approach is introduced here for the reconstruction of covariance matrix **M** and correlation times $\{\tau_m\}$ of a protein using heteronuclear spin relaxation parameters as input (Scheme 1) together with information obtained from molecular dynamics (MD) computer simulations. A key feature of the approach is

* To whom correspondence should be addressed. Phone: (508) 793-7220. Fax: (508) 793-8861. E-Mail: bruschweiler@nmr.clarku.edu.

(1) Abragam, A. *Principles of Nuclear Magnetism*; Clarendon Press: Oxford, 1961.
(2) Brüschweiler, R.; Case, D. A. *Prog. Nucl. Magn. Reson. Spectrosc.* **1994**, *26*, 27−58.
(3) Korzhnev, D. M.; Billeter, M.; Arseniev, A. S.; Orekhov, V. Y. *Prog. Nucl. Magn. Reson. Spectrosc.* **2001**, *38*, 197−266.
(4) Palmer, A. G. *Curr. Opin. Struct. Biol.* **1997**, *7*, 732−737.
(5) Kay, L. E. *Nat. Struct. Biol.* **1998**, *5*, 513−517.
(6) Ishima, R.; Torchia, D. A. *Nat. Struct. Biol.* **2000**, *7*, 740−743.
(7) Akke, M.; Brüschweiler, R.; Palmer, A. G. *J. Am. Chem. Soc.* **1993**, *115*, 9832−9833. Stone, M. *Acc. Chem. Res.* **2001**, *34*, 379−388. Spyracopoulos, L.; Sykes, B. D. *Curr. Opin. Struct. Biol.* **2001**, *11*, 555−559. Wand, A. J. *Nat. Struct. Biol.* **2001**, *8*, 926−931.
(8) Prompers, J. J.; Brüschweiler, R. *J. Am. Chem. Soc.* **2001**, *123*, 7305−7313.

10.1021/ja012750u CCC: $22.00

that it does not rely on the separability of internal and overall protein motions, which makes it equally well suited for the comprehensive motional characterization of folded, partially folded, and unfolded protein systems.

Heteronuclear relaxation data simultaneously reflect the rate of change of the protein orientation with respect to the external magnetic field and rates and amplitudes of protein structure changes. For globular proteins with a compact structure, internal motions do not markedly alter the protein shape, and they are often assumed to be separable from overall reorientational motion in good approximation. As a consequence, the relaxation data can be interpreted separately in terms of overall and internal motional effects which represents a convenient conceptual simplification. This separability assumption forms the basis of some of the most popular approaches of relaxation data interpretation including the Lipari−Szabo model-free approach[9] and its extension,[10] analytical motional models,[11,12] and approaches based on computer simulations.[2,3] In all these approaches, separability is exploited as follows. A model is derived for the internal correlation function, while an analytical expression is used for the overall tumbling correlation function. The latter is typically modeled as an isotropic or anisotropic reorientational diffusion process. In the case of isotropic overall tumbling, the overall tumbling part is a monoexponential function, and the total correlation function is simply the product of the internal and the overall correlation functions, $C_{tot}(t) = C_{overall}(t) \cdot C_{int}(t)$. The spectral-density mapping approach[13−15] does not require separability at the first place, but often involves such assumption when the spectral densities are interpreted in terms of motional amplitudes and time scales.

Relaxation data can also be interpreted using molecular dynamics (MD) computer simulations.[16−23] For long MD trajectories of small solutes that extensively sample overall tumbling motion, the separability of internal and overall motion can be assessed by comparison of the correlation functions $C_{tot}(t)$ and $C_{overall}(t) \cdot C_{int}(t)$ directly calculated from the trajectory.[24] However, due to the restricted lengths of current MD trajectories, overall reorientational motion of large and slowly tumbling biomolecules is usually inadequately sampled. To obtain the internal time-correlation functions, a commonly used procedure first eliminates overall reorientational motion from the trajectory by aligning each MD conformation (snapshot) with respect to a reference structure. From the modified trajectory, internal time-correlation functions are computed. The total correlation function is then calculated by multiplication with the overall tumbling correlation function (see above). The overall tumbling correlation times are determined from experimental data or estimated from hydrodynamic theory[3,25] or by combining MD simulations with a numerical solution of the overall tumbling diffusion equation. The latter method, termed mode-coupling Smoluchowski dynamics, has been applied to relaxation data of protein and DNA systems.[26−29]

NMR relaxation spectroscopy offers unique opportunities to study proteins that are partially folded or unfolded.[30−36] A detailed characterization of such states provides useful insights into the properties of protein folding intermediates and the protein folding process itself. Furthermore, it has been estimated that up to 30% of the human genome encodes for proteins that are natively unfolded or partially folded.[37,38] Because for highly flexible systems a molecular reference frame that defines the orientation of the molecule with respect to the laboratory frame does not exist, separability of overall and internal motion is not fulfilled. Consequently, NMR relaxation data interpretation becomes more difficult. NMR relaxation data of such systems are often converted to spectral density components[32,33,35,39] or interpreted on a residue-by-residue basis by an extended model-free approach,[10] which includes multiple order parameters and correlation times.[30,33,34] Alternatively, a continuous distribution of correlation times can be fitted to the relaxation data,[36,40] which is closely related to approaches commonly applied to relaxation data of synthetic polymers in solution and supercooled liquids.[41]

Individual protein atoms do not move independently with respect to each other, but rather in a correlated fashion involving atom groups of variable sizes.[42] Similarly, reorientations of bond vectors $\Omega_j(t)$ can exhibit significant amounts of correlation even after overall tumbling motion is subtracted.[43] A collective

(9) Lipari, G.; Szabo, A. *J. Am. Chem. Soc.* **1982**, *104*, 4546−4559. Lipari, G.; Szabo, A. *J. Am. Chem. Soc.* **1982**, *104*, 4559−4570.
(10) Clore, G. M.; Szabo, A.; Bax, A.; Kay, L. E.; Driscoll, P. C.; Gronenborn, A. M. *J. Am. Chem. Soc.* **1990**, *112*, 4989−4991.
(11) Woessner, D. E. *J. Chem. Phys.* **1962**, *36*, 1−4.
(12) Daragan, V. A.; Mayo, K. H. *Prog. Nucl. Magn. Reson. Spectrosc.* **1997**, *32*, 63−105.
(13) Peng, J. W.; Wagner, G. *J. Magn. Reson.* **1992**, *98*, 308−332. Peng, J. W.; Wagner, G. *Biochemistry* **1992**, *31*, 8571−8586. Peng, J. W.; Wagner, G. *Biochemistry* **1995**, *34*, 16733−16752.
(14) Farrow, N. A.; Zhang, O.; Szabo, A.; Torchia, D. A.; Kay, L. E. *J. Biomol. NMR* **1995**, *6*, 153−162.
(15) Ishima, R.; Nagayama, K. *J. Magn. Reson., Ser. B* **1995**, *108*, 73−76.
(16) Palmer, A. G.; Case, D. A. *J. Am. Chem. Soc.* **1992**, *114*, 9059−9067.
(17) Chandrasekhar, I.; Clore, G. M.; Szabo, A.; Gronenborn, A. M.; Brooks, B. *J. Mol. Biol.* **1992**, *226*, 239−250.
(18) Kördel, J.; Teleman, O. *J. Am. Chem. Soc.* **1992**, *114*, 4934−4936.
(19) Schmidt, J. M.; Brüschweiler, R.; Ernst, R. R.; Dunbrack, R. L.; Joseph, D.; Karplus, M. *J. Am. Chem. Soc.* **1993**, *115*, 8747−8756.
(20) Fushman, D.; Ohlenschläger, O.; Rüterjans, H. *J. Biomol. Struct. Dyn.* **1994**, *4*, 61−78.
(21) Chatfield, D. C.; Szabo, A.; Brooks, B. R. *J. Am. Chem. Soc.* **1998**, *120*, 5301−5311.
(22) Lienin, S. F.; Bremi, T.; Brutscher, B.; Brüschweiler, R.; Ernst, R. R. *J. Am. Chem. Soc.* **1998**, *120*, 9870−9879.
(23) Pfeiffer, S.; Fushman, D.; Cowburn, D. *J. Am. Chem. Soc.* **2001**, *123*, 3021−3036.
(24) Peter, C.; Daura, X.; van Gunsteren, W. F. *J. Biomol. NMR* **2001**, *20*, 297−310.
(25) Venable, R. M.; Pastor, R. W. *Biopolymers* **1988**, *27*, 1001−1014.
(26) La Penna, G.; Mormino, M.; Pioli, F.; Perico, A.; Fioravanti, R.; Gruschus, J. M.; Ferretti, J. A. *Biopolymers* **1999**, *49*, 235−254.
(27) La Penna, G.; Pratolongo, R.; Perico, A. *Macromolecules* **1999**, *32*, 2, 506−513.
(28) Fausti, S.; La Penna, G.; Cuniberti, C.; Perico, A. *Biopolymers* **1999**, *50*, 613−629.
(29) La Penna, G.; Fausti, S.; Perico, A.; Ferretti, J. A. *Biopolymers* **2000**, *54*, 89−103.
(30) Alexandrescu, A. T.; Shortle, D. *J. Mol. Biol.* **1994**, *242*, 527−546.
(31) Frank, M. K.; Clore, G. M.; Gronenborn, A. M. *Protein Sci.* **1995**, *4*, 2605−2615.
(32) Farrow, N. A.; Zhang, O.; Forman-Kay, J. D.; Kay, L. E. *Biochemistry* **1995**, *34*, 868−878.
(33) Buck, M.; Schwalbe, H.; Dobson, C. M. *J. Mol. Biol.* **1996**, *257*, 669−683.
(34) Brutscher, B.; Brüschweiler, R.; Ernst, R. R. *Biochemistry* **1997**, *36*, 13043−13053.
(35) Eliezer, D.; Chung, J.; Dyson, H. J.; Wright, P. E. *Biochemistry* **2000**, *39*, 2894−2901.
(36) Buevich, A. V.; Shinde, U. P.; Inouye, M.; Baum, J. *J. Biomol. NMR* **2001**, *20*, 233−249.
(37) Wright, P. E.; Dyson, J. E. *J. Mol. Biol.* **1999**, *293*, 321−331.
(38) Dunker, A. K.; Lawson, J. D.; Brown, C. J.; Williams, R. M.; Romero, P.; Oh, J. S.; Oldfield, C. J.; Campen, A. M.; Ratliff, C. M.; Hipps, K. W.; Ausio, J.; Nissen, M. S.; Reeves, R.; Kang, C.; Kissinger, C. R.; Bailey, R. W.; Griswold, M. D.; Chiu, W.; Garner, E. C.; Obradovic, Z. *J. Mol. Graphics* **2001**, *19*, 26−59.
(39) Viles, J. H.; Donne, D.; Kroon, G.; Prusiner, S. B.; Cohen, F. E.; Dyson, H. J.; Wright, P. E. *Biochemistry* **2001**, *40*, 2743−2753.
(40) Buevich, A. V.; Baum, J. *J. Am. Chem. Soc.* **1999**, *121*, 8671−8672.
(41) Rössler, E.; Sillescu, H. Organic Glasses and Polymers. In *Materials Science and Technology*; Zarzycki, J., Ed.; VCH: Weinheim, 1991; Vol. 9, pp 573−618.
(42) Brooks, C. L., III; Karplus, M.; Pettitt, B. M. *Proteins: A Theoretical Perspective of Dynamics, Structure, and Thermodynamics*; John Wiley & Sons: New York, 1988.
(43) Lienin, S. F.; Brüschweiler, R. *Phys. Rev. Lett.* **2000**, *84*, 5439−5442.

description of NMR relaxation-active motions has recently been introduced in terms of reorientational eigenmode dynamics (RED) for data interpretation of a mobile loop region of native ubiquitin.[8] This approach incorporates motional correlations between reorientations of backbone N−H bonds in the form of a covariance matrix of spherical harmonics of rank 2 calculated from a MD trajectory. For molecules for which internal motions are separable from overall motions, the covariance matrix of the RED approach is expressed in a molecule-fixed frame. The reorientational eigenmodes and the amplitudes are determined by diagonalization of the covariance matrix with each eigenmode possessing its internal correlation time.[8]

For more mobile systems, a new situation arises. For example, for the partially folded A-state of ubiquitin obtained in a methanol−water mixture, which is discussed in this paper, large-amplitude reorientational motions of backbone N−H vectors are observed during MD simulations. While for a 5 ns segment of the trajectory overall motion can still be approximately eliminated by aligning each snapshot with respect to a reference structure,[44] for significantly longer simulation times such an alignment procedure is elusive since a wide range of internal conformations is sampled and a suitable reference structure does not exist any longer. Moreover, overall reorientational motion of the A-state is statistically not well sampled by the MD trajectory even for simulation times in the tens of nanosecond range. Thus, correlation functions have nonnegligible statistical uncertainties, which impedes direct comparison of NMR relaxation parameters back-calculated directly from the trajectory with experimental data.

The approach introduced here does not require separability of internal and overall motion. Similar to the RED concept, it is based on a covariance matrix analysis of internuclear vector orientations, represented by spherical harmonics, extracted from a MD trajectory. The length of presently feasible trajectories usually precludes that the conformational ensemble is isotropic, that is, that each internal conformation is represented by a large number of snapshots with an isotropic orientational distribution. The new approach, termed isotropic reorientational eigenmode dynamics analysis (iRED), overcomes this limitation by analytically integrating each snapshot over an isotropic distribution of orientations. The resulting eigenmodes and amplitudes, which reflect both overall tumbling and reorientational internal motions, allow the quantitative assessment of the separability of the two types of motions. By adjusting correlation times belonging to large-amplitude eigenmodes, the agreement between theory and experiment can be optimized. The iRED analysis is applied here to two states of ubiquitin that exhibit vastly different flexibility: the globular native state and the partially folded A-state.

2. Theory

The main theoretical results of the iRED method are summarized in this section. Derivations and further explanations can be found in Appendices A1−A6. According to the relaxation theory of Bloch, Wangsness, and Redfield,[45,46] spin relaxation parameters T_1, T_2, and NOE are determined by the spectral density functions $J_j(\omega)$ (see Appendix A1)

$$J_j(\omega) = \int_{-\infty}^{\infty} C_j(t) \cos \omega t \, dt \tag{1}$$

where $C_j(t)$ is the time-correlation function of the lattice part of the spin interaction that causes relaxation

$$C_j(t) = \langle Y_{LM}(\Omega_j(\tau)) Y_{LM}^*(\Omega_j(\tau + t)) \rangle_\tau \tag{2}$$

where $Y_{LM}(\Omega_j)$ are the spherical harmonics of rank L evaluated at directions Ω_j of internuclear vector j, and $M = -L, ..., L$. The angular brackets indicate averaging over time τ.

Because the lattice parts of dominant NMR relaxation−active interactions, such as the magnetic dipole−dipole interaction and the chemical shielding anisotropy (CSA), can be expressed in terms of spherical harmonics of rank 2, the covariance matrix with $L = 2$ will be particularly relevant in the following discussion. On the other hand, the rank $L = 1$ case, which corresponds to the reorientation of three-dimensional unit vectors, is more intuitive.[43] Therefore, expressions are given for general L values. Spin relaxation measurements are usually performed in isotropic protein solutions, which means that each internal conformation has the same overall orientational probability. As a consequence, $C_j(t)$ does not depend on M (see, e.g., ref 2).

We consider the evaluation of eqs 1 and 2 from a molecular dynamics (MD) or Monte Carlo trajectory of a protein of total length T consisting of N conformations (snapshots). For a conformation sampled at time t, the principal-axis directions $\Omega_j(t) = (\theta_j(t), \varphi_j(t))$, $j = 1, ..., n$, of the n dipolar interactions of interest (or of other relaxation−active interactions such as chemical shielding anisotropy) are extracted. During the simulation, the orientation of the protein is not fixed; that is, the protein is allowed to undergo free rotational tumbling. For the subsequent analysis, the snapshots do not need to be orientationally aligned with respect to a reference structure. In contrast to the experimental situation, a MD trajectory of finite length will generally produce an anisotropic reorientational distribution, which would lead to a dependence of $C_j(t)$ on M.

In the iRED method, the covariance matrix of the $Y_{LM}(\Omega_j(t))$ functions is calculated from the trajectory. In a subsequent step, the covariance matrix is isotropically averaged over all possible orientations of each snapshot (for a mathematical treatment see Appendix A2). The spherical symmetry introduced by the isotropic averaging leads to a substantial simplification of the covariance matrix with all relevant information contained in the real symmetric $n \times n$ matrix $\mathbf{M}$ with elements

$$M_{kl} = \overline{P_L(\cos(\Omega_k - \Omega_l))} \tag{3}$$

where $P_L(x)$ is the Legendre polynomial of order L ($P_1(x) = x$, $P_2(x) = (3x^2 - 1)/2$, etc.), $\Omega_k - \Omega_l$ denotes the angle between directions Ω_k and Ω_l taken from the same snapshot, and the horizontal bar indicates averaging over all snapshots of the trajectory.[47]

(44) Prompers, J. J.; Scheurer, C.; Brüschweiler, R. *J. Mol. Biol.* **2001**, *305*, 1085−1097.
(45) Wangsness, R. K.; Bloch, F. *Phys. Rev.* **1953**, *89*, 728−739. Bloch, F. *Phys. Rev.* **1956**, *102*, 104−135.
(46) Redfield, A. G. *IBM J. Res. Dev.* **1957**, *1*, 19−31. Redfield, A. G. *Adv. Magn. Reson.* **1965**, *1*, 1−32.

(47) $M_{kl} = \overline{P_L(\cos(\Omega_k - \Omega_l))}$ should not be confused with the generalized order parameter S^2 that can be calculated from a MD trajectory according to $S^2 = \langle P_2(\cos(\Omega_i - \Omega_j)) \rangle_{ij}$, where all snapshots are orientationally aligned with respect to a reference snapshot, and where $\Omega_i - \Omega_j$ is the orientational change of the internuclear vector when going from snapshot i to snapshot j.

The reorientational eigenmodes and their amplitudes are the eigenvectors $|m\rangle$ and eigenvalues λ_m of $\mathbf{M}$ fulfilling $\mathbf{M}|m\rangle = \lambda_m|m\rangle$ (Appendix A2). The eigenmodes describe correlated modulations of different spin interactions, and the eigenvalues correspond to the variances of the amplitude fluctuations of the trajectory along each eigenmode. The eigenvalues fulfill $\lambda_m \geq 0$, and their sum is equal to the number of spin interactions n. Covariance matrix $\mathbf{M}$ plays a key role in NMR relaxation representing in a condensed form all spatial aspects of motional information obtainable from spin relaxation experiments of an isotropic protein sample. In contrast to the RED approach,[8] for the computation of the reorientational covariance matrix $\mathbf{M}$, no assumption about the existence of a molecular reference frame is made in which internal and overall motions are separable in a statistical sense. The eigenmodes and eigenvalues depict these motions in terms of amplitudes and motional correlation effects experienced by the different spin interactions. For an internally rigid molecule, covariance matrix $\mathbf{M}$ has at most $2L + 1$ nonzero eigenvalues. The corresponding eigenmodes do not reflect internal dynamics, and they can be used to model overall reorientational motion.

In matrix $\mathbf{M}$, the time-sequence information of the original MD trajectory has been lost; therefore $\mathbf{M}$ contains no information on motional correlation times associated with individual reorientational modes $|m\rangle$ or information about anisotropic rotational tumbling. Such information can be obtained by calculating time-correlation functions $C_m(t)$ from time-dependent amplitudes $a_{m,l}(t)$ that are obtained by projecting MD snapshots on the eigenmodes (Appendix A3):

$$C_m(t) = \sum_{l=-L}^{L} \langle a_{m,l}^*(\tau + t) \cdot a_{m,l}(\tau) \rangle_\tau \qquad (4)$$

where the average extends over the trajectory. Correlation times τ_m of these correlation functions can be determined by exponential fitting (Appendix A3).

For the systems studied here, the $C_m(t)$ are found to decay in good approximation monoexponentially (see Application sections). In this case, the spectral density function $J(\omega)$ of eq 1 can be analytically expressed as

$$J_j(\omega) = \int_{-\infty}^{\infty} C_j(t) \cos \omega t \, dt = \sum_m \delta S_{j,m}^2 \frac{2\tau_m}{1 + \omega^2 {\tau_m}^2} \qquad (5)$$

where $\delta S_{j,m}^2 = \lambda_m ||m\rangle_j|^2$ are the *principal order parameter components* corresponding to the decay of $C_j(t)$ due to mode m. More details can be found in Appendix A4. If overall and internal motions are separable, the Lipari−Szabo S_j^2 order parameter of interaction j is given by

$$1 - S_j^2 = \sum_{m'} \delta S_{j,m'}^2 \qquad (6)$$

where the sum extends only over internal modes m'.

Calculated and experimental relaxation parameters are quantitatively compared as usual by

$$\chi^2 = \sum_i \frac{(X_i^{\text{calc}} - X_i^{\text{exp}})^2}{\sigma_i^2} \qquad (7)$$

where X_i^{calc} are the calculated and X_i^{exp} the experimental T_1, T_2, and NOE parameters, and σ_i are the corresponding experimental errors. As described below, the correlation times τ_m can be adjusted to minimize χ^2 using a least-squares fitting procedure.

3. MD Simulations

Two MD simulations were performed under periodic boundary conditions using the program CHARMM.[48,49] The first trajectory corresponds to native ubiquitin, and the second one corresponds to a partially folded state of ubiquitin. For the native trajectory, an all-atom representation of the X-ray structure of ubiquitin[50] was embedded in a cubic box including 2909 explicit water molecules. The simulation was performed at a temperature of 300 K for 6 ns. More details on the trajectory are described elsewhere.[22,44] The first 1 ns of the MD simulation was used for equilibration, and a total of 1000 snapshots with a time increment of 5 ps were analyzed from the final 5 ns of the trajectory (segment 1−6 ns).

For the trajectory of the partially folded state, ubiquitin was simulated under the conditions experimentally known to induce the A-state, that is, a 60%/40% (v/v) methanol/water mixture at low pH.[34,57,58] An all-atom representation of the protein was protonated and immersed in a cubic box containing a total of 1727 water molecules and 1102 methanol molecules. During the first part of the 70 ns trajectory, the temperature was varied to guide and to speed-up the conformational transformation of the native state into a state resembling the A-state, while the final 42.8 ns (segment 27.2−70.0 ns) of the trajectory were performed at 300 K. An analysis of the first 33 ns of this simulation has been reported elsewhere.[44] In the present work, 800 snapshots of the final 40 ns of the trajectory corresponding to the segment starting at 30 ns and ending at 70 ns sampled at a time increment of 50 ps were used for analysis.

4. Application to Native Ubiquitin

Isotropic RED Analysis of Rank 1. Characteristic features of the iRED method can be demonstrated for the rank $L = 1$ case applied to the 6 ns MD simulation of the native state of ubiquitin. During the simulation, ubiquitin is stable and retains a highly globular character with a radius of gyration $R_g = 11.67 \pm 0.08$ Å. An iRED analysis of rank 1 was performed on the

(48) Brooks, R. B.; Bruccoleri, R. E.; Olafson, B. D.; States, D. J.; Swaminathan, S.; Karplus, M. *J. Comput. Chem.* **1983**, *4*, 187−217.
(49) MacKerell, A. D., Jr.; Bashford, D.; Bellott, M.; Dunbrack, R. L., Jr.; Evanseck, J. D.; Field, M. J.; Fischer, S.; Gao, J.; Guo, H.; Ha, S.; Joseph-McCarthy, D.; Kuchnir, L.; Kuczera, K.; Lau, F. T. K.; Mattos, C.; Michnick, S.; Ngo, T.; Nguyen, D. T.; Prodhom, B.; Reiher, W. E., III; Roux, B.; Schlenkrich, M.; Smith, J. C.; Stote, R.; Straub, J.; Watanabe, M.; Wiórkiewicz-Kuczera, J.; Yin, D.; Karplus, M. *J. Phys. Chem. B* **1998**, *102*, 3586−3616.
(50) Vijay-Kumar, S.; Bugg, C. E.; Cook, W. J. *J. Mol. Biol.* **1987**, *194*, 531−544.
(51) Schneider, D. M.; Dellwo, M. J.; Wand, A. J. *Biochemistry* **1992**, *31*, 3645−3652.
(52) Tjandra, N.; Feller, S. E.; Pastor, R. W.; Bax, A. *J. Am. Chem. Soc.* **1995**, *117*, 12562−12566.
(53) Lienin, S. F. Anisotropic Dynamics in Molecular Systems Studied by NMR Relaxation, ETH Thesis No. 12871, Zürich, 1998.
(54) Ottiger, M.; Bax, A. *J. Am. Chem. Soc.* **1998**, *120*, 12334−12341.
(55) Case, D. A. *J. Biomol. NMR* **1999**, *15*, 95−102.
(56) Woessner, D. E. *J. Chem. Phys.* **1962**, *37*, 647−654.
(57) Wilkinson, K. W.; Mayer, A. N. *Arch. Biochem. Biophys.* **1986**, *250*, 390−399.
(58) Stockman, B. J.; Euvrard, A.; Scahill, T. A. *J. Biomol. NMR* **1993**, *3*, 285−296.

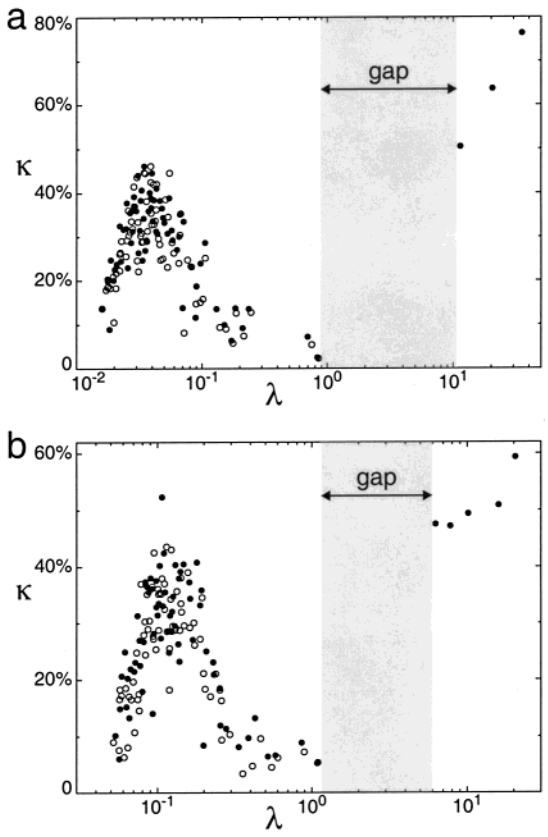

Figure 1. Mode collectivities κ vs eigenvalues λ for the RED and the isotropic RED analyses performed on the 72 backbone N−H vectors of native ubiquitin using (a) Cartesian vectors (equivalent to rank $L = 1$ spherical harmonics) and (b) rank $L = 2$ spherical harmonics. The results for the isotropic RED analyses are shown as filled circles, and the results for the standard RED analyses are shown as open circles. κ, which can vary between 1.4% and 100%, is a measure for the relative number of N−H vectors that are significantly affected by a given mode.

72 backbone N−H vectors (excluding the N-terminal residue) using 1000 snapshots from the final 5 ns of the MD simulation. For comparison, a standard RED analysis[8] was carried out on the same vectors after overall translational and reorientational motions were removed by a least-squares superposition of each snapshot, including backbone and side-chain atoms, with respect to the "half-time" snapshot at 3.5 ns.

A convenient way to visualize the separability of overall and internal motions is shown in Figure 1a by plotting the mode collectivities κ versus the eigenvalues λ for the two analyses. κ gives the percentage of interactions significantly affected by a given mode calculated according to eq A25, while λ represents the variance of the amplitude fluctuation of the trajectory along this mode. The iRED analysis exhibits three very large amplitude modes with high collectivities indicating that between 51% and 76% of all backbone N−H vectors are significantly affected by these reorientational modes. They predominantly reflect rigid-body overall rotational motion, and they are separated from all other modes by a large gap in the mode amplitudes λ. The larger the gap, the better separable are the overall and internal motions. A quantitative measure for the gap magnitude is the separability index $g_1 = 14.05$, which is defined in eq A26. There is also a gap in collectivities κ between the overall tumbling modes ($\kappa > 50\%$) and the largest internal modes ($\kappa < 20\%$).

In contrast, for the standard RED analysis, which operates on aligned snapshots, the overall reorientational modes disappear, and the internal modes are only slightly changed both in the mode amplitudes λ and in the collectivities κ. Thus, the alignment procedure effectively removes overall motions. Therefore, overall and internal motions are separable in good approximation as is expected for this globular protein system exhibiting a well-defined structure undergoing restricted internal motion. As noted previously,[43,44] the internal mode collectivities κ of this globular protein exhibit a characteristic distribution as a function of λ with some of the lowest collectivities belonging to the smallest and the largest amplitude modes.

The three largest eigenvalues of the iRED analysis vary significantly: $\lambda_{70} = 11.36$, $\lambda_{71} = 20.40$, $\lambda_{72} = 35.12$. They do not contain information about isotropic or anisotropic overall tumbling motion, but rather reflect the anisotropy of the orientational distribution of the average directions of the N−H vectors. It can be shown using distance geometry theory[59] that the average orientations of the internuclear vectors are determined by the eigenvectors and eigenvalues.[60]

Isotropic RED Analysis of Rank 2. The iRED and standard RED analyses were performed on the same snapshots for rank 2 spherical harmonics with the resulting mode collectivities κ and eigenvalues λ shown in Figure 1b. In contrast to the rank 1 case, there are now five overall rotational modes for the iRED analysis. The separability index is $g_2 = 6.30$ (eq A26), which is less than one-half of the g_1 value of the rank 1 case. Amplitudes and collectivities of internal modes are again similar for iRED and standard RED, and they qualitatively follow the same distribution as for the rank 1 case of Figure 1a.

Each mode m yields, according to eq 5, a Lorentzian contribution to the spectral density $J_j(\omega)$ of interaction j determined by the principal order parameter component $\delta S^2_{j,m}$ with correlation time τ_m. The $\delta S^2_{j,m}$ components of the 10 modes with largest amplitudes λ_m are shown in Figure 2. The overall reorientational modes $m = 68, ..., 72$ are highly collective affecting a large portion of all N−H vectors in a correlated fashion. In contrast, the five largest internal modes $m = 63, ..., 67$ have a much more local character and mainly affect the C-terminal end and residues belonging to loop regions.

For the iRED analysis of rank 2, the correlation times τ_m of protein motions along the reorientational eigenmodes can be estimated from the time-correlation functions $C_m(t)$ calculated for each mode using eqs A17−A19. The $C_m(t)$ follow for the five largest internal modes $m = 63, ..., 67$ in good approximation a monoexponential decay, as is the case for most of the other internal modes, and their correlation times τ_m can be determined using eq A19. As is discussed in Appendix A3 and in the Supporting Information, the τ_m values of the internal modes correspond to effective correlation times rather than internal correlation times τ_m'. The τ_m values are slightly shorter than the τ_m' values due to the overall tumbling in accordance with eq A21.

The correlation functions of the five overall reorientational modes $m = 68, ..., 72$ have not converged during the 5 ns simulation. Therefore, reliable estimates of their correlation times τ_m cannot be made from the trajectory. The extracted τ_m

(59) Crippen, G. M.; Havel, T. F. *Distance Geometry and Molecular Conformation*; Research Studies Press: Letchworth, U.K., 1988.
(60) Prompers, J. J.; Brüschweiler, R. *Proteins* **2002**, *46*, 177−189.

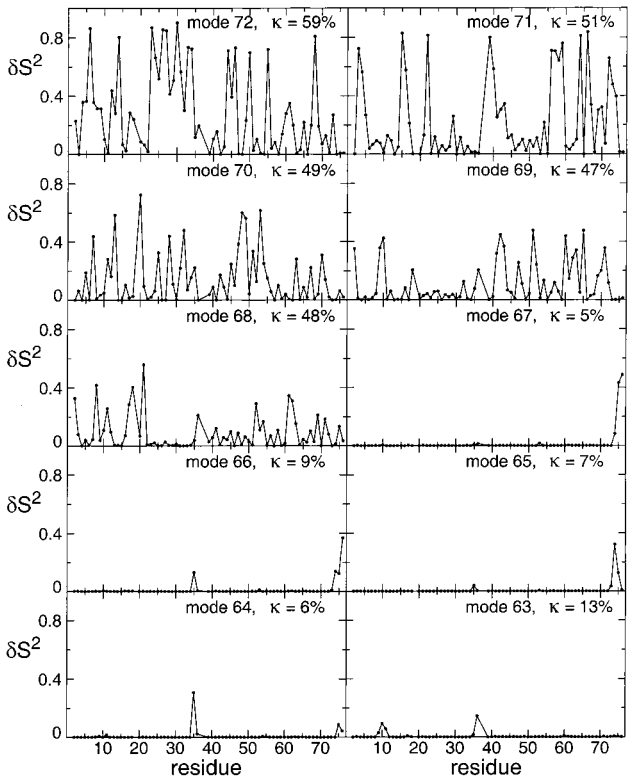

Figure 2. Reorientational mobilities of backbone N−H vectors of native ubiquitin expressed in terms of principal order parameter components $\delta S^2_{j,m}$ of reorientational modes $m = 63, ..., 72$ derived from the covariance matrix **M** (eq 3).

Table 1. Correlation Times for the Native State

	original MD	fitted[a]
τ_{72} (ns)	0.59	4.12 ± 0.03
τ_{71} (ns)	0.66	3.93 ± 0.02
τ_{70} (ns)	0.65	4.27 ± 0.04
τ_{69} (ns)	0.53	4.27 ± 0.07
τ_{68} (ns)	0.44	3.89 ± 0.08
τ_{67} (ps)	490	165 ± 5
τ_{66} (ps)	423	0.1 ± 0.3
τ_{65} (ps)	369	631 ± 4
τ_{64} (ps)	368	3344 ± 84
τ_{63} (ps)	172	4446 ± 370

[a] Standard deviations determined from a Monte Carlo error analysis consisting of 50 simulations.

values are clearly shorter than the experimentally determined overall tumbling correlation times of ubiquitin (Table 1). The distribution of the original τ_m values is depicted in the Supporting Information.

Fitting of iRED Parameters to Experimental Data. Several sets of backbone ^{15}N relaxation data of native ubiquitin have been reported in the literature.[22,51,52] In the following analysis backbone, ^{15}N T_1 relaxation times and $\{^1$H$\}$-^{15}N heteronuclear NOEs collected at 400 and 600 MHz magnetic field strengths and ^{15}N T_2 relaxation times measured at 600 MHz were taken from Table 1 of the Supporting Information of Lienin et al.[22] All data were collected at 300 K, and they are displayed as filled circles in Figure 3. Estimates of the statistical uncertainty of the experimental data, that had been obtained by repeating the experiments, are as follows:[22,53] the standard deviations

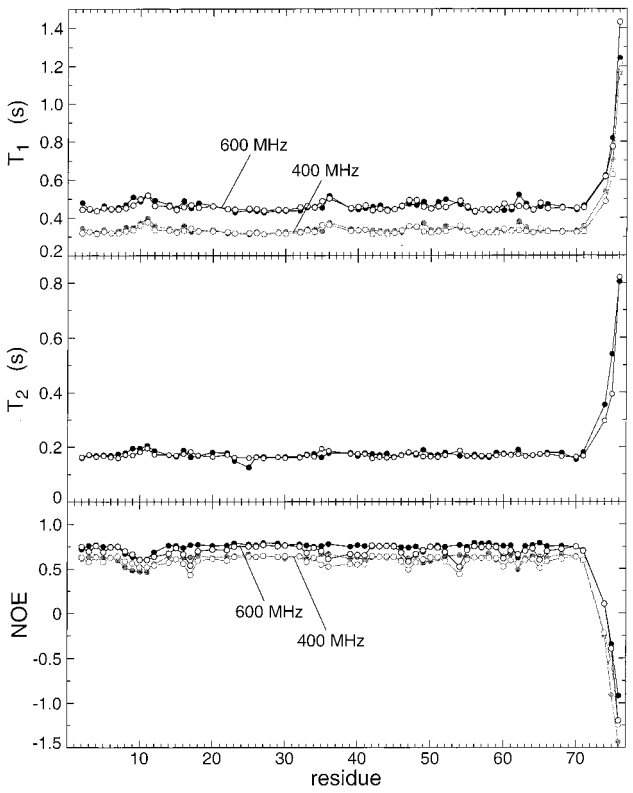

Figure 3. ^{15}N T_1 and T_2 relaxation times and $\{^1$H$\}$-^{15}N NOEs at 600 MHz (black circles) and 400 MHz (gray circles) proton frequency for native ubiquitin. Experimental relaxation parameters[22] are shown as filled circles. Relaxation parameters calculated using the iRED analysis of rank 2 applied to the 5 ns native MD trajectory after fitting the correlation times of the 10 largest modes $m = 63, ..., 72$ are shown as open circles.

are 1.5% for T_1 values at 400 and 600 MHz, 4% for NOEs at 400 MHz, 2.5% for NOEs at 600 MHz, and 2% for T_2 values at 600 MHz.

^{15}N T_1, T_2, and NOE relaxation parameters were calculated from the iRED analysis of the 1−6 ns segment of the trajectory. The spectral density functions were determined according to eq 5 and inserted into the expressions for T_1, T_2, and NOE given in Appendix A1. Dipolar relaxation contributions were determined using a N−H bond length of $r_{NH} = 1.04$ Å,[54,55] and CSA contributions were computed using an axially symmetric ^{15}N CSA tensor with the symmetry axis parallel to the N−H vector and with an asymmetry $\Delta\sigma = -176$ ppm. The calculated values qualitatively reproduce most of the trends, but they have a large offset as compared to the experimental relaxation parameters, which is caused primarily by the correlation times of the five overall reorientational modes estimated from the MD trajectory, which are too short, leading to a χ^2 value defined in eq 7 of 3.23×10^6.

To improve agreement between iRED results and experimental relaxation data, correlation times of the reorientational eigenmodes were adjusted. First, only correlation times τ_m of the five largest, overall reorientational modes $m = 68, ..., 72$ were adjusted by a nonlinear least-squares fitting procedure, which causes an increase of the correlation times by nearly an order of magnitude to values around 4 ns. The χ^2 value improves by almost a factor of 100 ($\chi^2 = 3.43 \times 10^4$). The effective overall tumbling correlation time τ_c, which is calculated as the average of $\tau_{68}, ..., \tau_{72}$, is 4.05 ns, which is very close to the

value of 4.03 ns determined using a model-free analysis of the same experimental data.[22]

Next, the five largest internal modes were also included in the fit by simultaneously adjusting the correlation times of the 10 largest modes $m = 63, ..., 72$. The χ^2 value drops by almost an order of magnitude to 3.71×10^3. The back-calculated relaxation parameters are displayed as open circles in Figure 3. For residues belonging to regular secondary structures (rigid core residues), the agreement is very good, and also for flexible regions, the data are well reproduced. Considering that only 10 fit parameters are used for the interpretation of a total of 310 relaxation parameters, the quality of the fit is remarkably good. The adjusted correlation times are given in Table 1 together with the original values. The effective τ_c value slightly increases to 4.10 ns remaining close to the model-free τ_c value. The correlation times $\tau_{68}, ..., \tau_{72}$ vary between 3.89 and 4.27 ns, which confirms earlier findings that native ubiquitin tumbles in good approximation isotropically.[52]

Overall tumbling anisotropy can be assessed by a more detailed analysis of the variations among the correlation times $\tau_{68}, ..., \tau_{72}$. Although these values depend also on the associated eigenmode directions, which do not necessarily coincide with the diffusion tensor principal axes, it is possible to obtain estimates for the principal axis values of the rotational diffusion tensor using Woessner's equations.[56] From the $\tau_{68}, ..., \tau_{72}$ values, the following diffusion tensor principal axis values are obtained: $D_{xx} = 37.4 \times 10^6\ s^{-1}$, $D_{yy} = 40.3 \times 10^6\ s^{-1}$, $D_{zz} = 44.1 \times 10^6\ s^{-1}$. A measure for the anisotropy of the diffusion tensor is $2D_{zz}/(D_{xx} + D_{yy}) = 1.14$, which compares well with the corresponding value of 1.16 found by Tjandra et al.[52] When the fitting is constrained such that modes $m = 68, ..., 72$ have all the same correlation time τ_c, the optimized τ_c value is 4.11 ns. The fitting results thereby change only little with χ^2 increasing by 9% to $\chi^2 = 4.04 \times 10^3$.

If the correlation times of the 15 largest modes ($m = 58, ..., 72$) are individually adjusted, the χ^2 value further decreases to $\chi^2 = 3.12 \times 10^3$. The correlation times of the 10 largest modes thereby remain close to the ones obtained from the fit using only 10 correlation times as variable parameters.

5. Application to the A-State of Ubiquitin

Structural Features. Analysis of the initial 33 ns of the trajectory of the partially folded state of ubiquitin[44] shows that during the 5 ns between 28 and 33 ns the N-terminal half of the simulated state is similar to the A-state experimentally characterized by circular dichroism[57] and NMR.[34,58] It contains a nativelike N-terminal antiparallel β-sheet and a central helix, but in contrast to the experimental studies and consistent with earlier MD work,[61] the simulation lacks helical propensity in the C-terminal half of the polypeptide chain. The trajectory used for the following iRED analysis was extended beyond the original 33 ns by an additional 37 ns leading to a total length of 70 ns. During the final 37 ns, no formation of helical structure is observed in the C-terminal half of the protein. Because of the qualitative differences in the C-terminal half between experimental and simulated properties, we decided to analyze the N-terminal half of ubiquitin (residues 1−29) whose structural dynamic properties qualitatively match the experimental findings.

(61) Alonso, D. O. V.; Daggett, V. *J. Mol. Biol.* **1995**, *247*, 501−520.

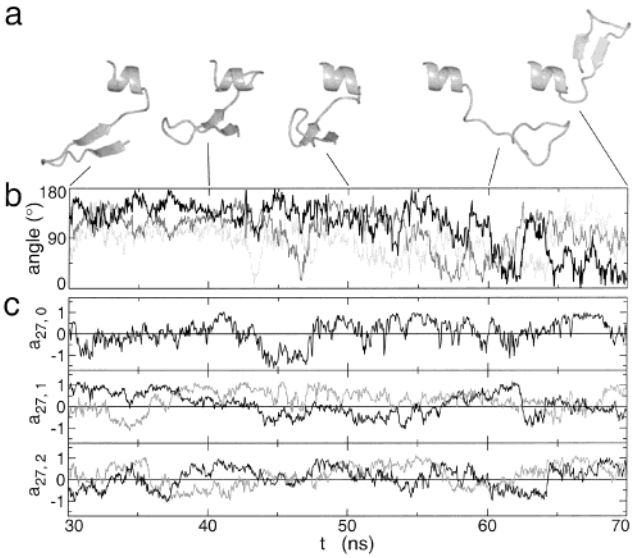

Figure 4. Reorientational motions of the helix with respect to the sheet in the A-state of ubiquitin. Panel a shows selected snapshots along the trajectory at 30, 40, 50, 60, and 70 ns. The structures were aligned on the C^α atoms of helix residues 22−28 of the snapshot at 30 ns, and ribbon representations were created with the program MOLMOL.[63] Panel b shows the angles as a function of simulation time between the helix axis (average of N−H vectors in the helix) and three orthogonal coordinate axes rigidly attached to the sheet (average of N−H vectors in the sheet (black line), axis perpendicular to average N−H vector in the plane of the sheet (dark gray line), and axis perpendicular to the plane of the sheet (light gray line)). Panel c shows projection coefficients $a_{m,l}(t)$ belonging to the largest mode $m = 27$: $a_{27,0}$ (upper panel), Re$\{a_{27,1}\}$ (middle panel, black line), Im$\{a_{27,1}\}$ (middle panel, gray line), Re$\{a_{27,2}\}$ (lower panel, black line), Im$\{a_{27,2}\}$ (lower panel, gray line).

During the final 40 ns of the MD simulation of the partially folded state of ubiquitin, the protein is highly dynamic and adopts a large range of conformations, including conformers that are compact and some that are more extended (see snapshots depicted in Figure 4a). The N-terminal β-sheet with residues 3, 4 and 14, 15 is quite stable between 30 and 50 ns, while it undergoes unfolding and refolding between 50 and 70 ns (Figure 4a). The central helix (residues 22−28), while always present, is somewhat unstable at its C-terminal end fluctuating between an α-helix and a π-helix.

Isotropic RED of Rank 2. The iRED analysis of rank 2 was applied to the 27 backbone N−H vectors of the N-terminal half of the A-state (residues 1−29, excluding Met 1 and Pro 19) using 800 snapshots from the final 40 ns of the A-state simulation with a time increment of 50 ps. The mode collectivities κ versus the eigenvalues λ are shown in Figure 5. For the partially folded state, there is no clear gap between the overall rotational modes and the internal modes, which is also reflected in a low separability index $g_2 = 2.51$. This behavior, which sharply contrasts the one of the native state (Figure 1), suggests that separability of internal and overall motions is clearly not fulfilled. The small separability index g_2 also indicates that no static structural model exists that is compatible with the covariance matrix **M**. Therefore, procedures for the back-calculation of relaxation parameters requiring alignment of each snapshot with respect to a reference structure are not suitable in this case.

The A-state results qualitatively differ from the native simulation also with respect to the collectivity properties of the

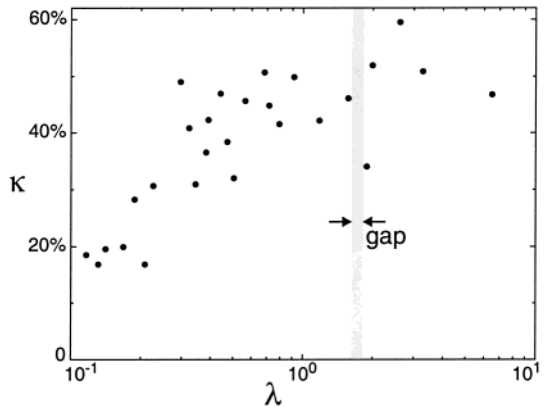

Figure 5. Mode collectivities κ vs eigenvalues λ for the iRED analysis of rank 2 performed on the 27 backbone N−H vectors of the N-terminal half of the A-state of ubiquitin.

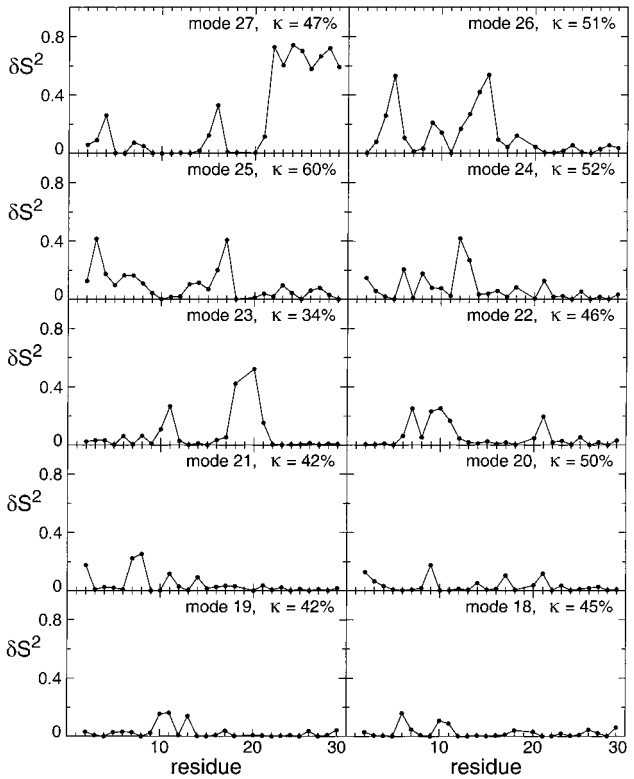

Figure 6. Reorientational mobilities of backbone N−H vectors of the N-terminal half of the A-state of ubiquitin expressed in terms of principal order parameter components $\delta S^2_{j,m}$ of reorientational modes $m = 18, ..., 27$ derived from covariance matrix **M** (eq 3).

high-amplitude modes as can be seen in Figure 5; the collectivities steadily increase with increasing λ without exhibiting a characteristic drop for the largest internal modes observed for native ubiquitin (Figure 1).[43] The principal order parameter components $\delta S^2_{j,m}$ for the 10 largest modes are displayed in Figure 6. These modes have notably high collectivities between 34% and 60%. The helix and the sheet are simultaneously affected only by modes 27 and 25, while all other modes predominantly involve the β-sheet and the hinge region. Mode 27 uniformly and strongly affects the helix and, to a lesser extent, selected parts of the β-sheet, while mode 25 modulates parts of the sheet more strongly than the helix. Modes 27 and 25 reflect what is left of the structural "long-range" order between the two secondary structural elements. The internally dynamic character of the β-sheet and the loop connecting the two strands is manifested in the form of the different subsets of N−H vectors involved in different modes.

The extent of reorientational motions of the helix with respect to the sheet during the simulation can be assessed from the angles between the helix axis, which is defined as the average orientation of all N−H vectors of the helix, and three orthogonal vectors rigidly attached to the sheet: one vector pointing along the average N−H vector orientation in the sheet, one perpendicular to the average N−H vector in the plane of the sheet, and one perpendicular to the plane of the sheet. These angles are displayed as a function of the simulation time in Figure 4b together with selected backbone structures aligned with respect to the helix (panel a). During the simulation, the sheet undergoes almost a 180° flip with respect to the helix. The projection coefficients $a_{27,l}(t)$ ($l = -2, ..., 2$) of the snapshots on the modes belonging to mode 27 of matrix **M** show significant modulations (Figure 4c). They also reflect the insensitivity of spherical harmonics of rank 2 with respect to the 180° flip as is manifested in similar projection coefficients at 40 and 70 ns.

This has direct implications for the convergence behavior of the principal order parameter components. Separate analysis of the 10 ns MD segment between 40 and 50 ns yields for the largest six modes a very similar behavior as the one observed in Figure 6. This indicates, consistent with Figure 4c, that the convergence of the covariance matrix is better than expected from the snapshots depicted in Figure 4a.

Correlation times τ_m were extracted from time-correlation functions $C_m(t)$ using eq A19. The modes decay in good approximation monoexponentially as is illustrated for the two correlation functions belonging to mode 27 and mode 20 of the A-state plotted in Figure 7. The distribution of all correlation times is given in the Supporting Information. All extracted correlation times are larger than 250 ps, indicating that for an increasing trajectory length fast structural fluctuations are dominated by slower time-scale events.

Fitting of Isotropic RED to Experimental Data. For the A-state, ^{15}N T_1 (at 400, 600, and 800 MHz) and T_2 (at 400 and 600 MHz) relaxation times and {^{1}H}-^{15}N heteronuclear NOEs (at 600 and 800 MHz) were taken from Table 2 of the Supporting Information of Brutscher et al.[34] All data were collected at 300 K, and they are shown for the N-terminal half of the protein as filled circles in Figure 8. Errors in the experimental data were estimated from the standard deviations of multiple measurements at 600 MHz and are in the range of $4 \pm 2\%$ for T_1, $9 \pm 4\%$ for T_2, and $7 \pm 4\%$ for the NOE, while duplicate recordings of NOE spectra at 800 MHz yielded a relative error of $2 \pm 1\%$.[34] The T_2 relaxation times of residues Thr 9 and Thr 12 were found to have exchange contributions,[34] and these data points were excluded from the analysis. This yields a total of 157 experimental relaxation parameters used for the following iRED analysis.

The ^{15}N T_1, T_2, and NOE relaxation parameters back-calculated from the trajectory (using eqs 5, A1−A3) without adjustment of correlation times cannot satisfactorily reproduce the experimental data as is reflected in a high χ^2 value of 1.42×10^4. Adjustment of the correlation times of the five largest modes $m = 23, ..., 27$ leads to a significant improvement ($\chi^2 = 2.54 \times 10^3$), and adjustment of the correlation times of the 10

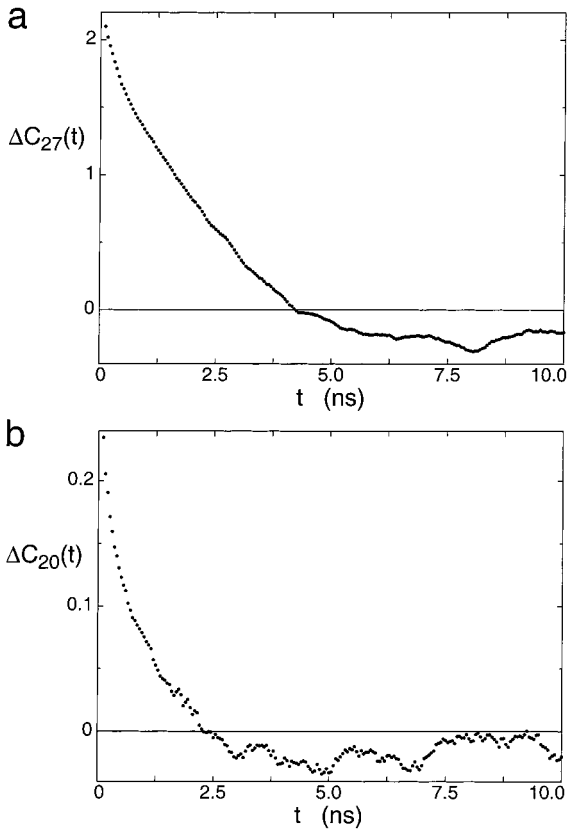

Figure 7. Time-correlation functions $\Delta C_m(t) = C_m(t) - C_m(t \rightarrow T)$ calculated according to eqs A17, A18 of two selected reorientational eigenmodes $m = 27$ and $m = 20$ of the N-terminal half of the A-state of ubiquitin derived from covariance matrix **M** (eq 3).

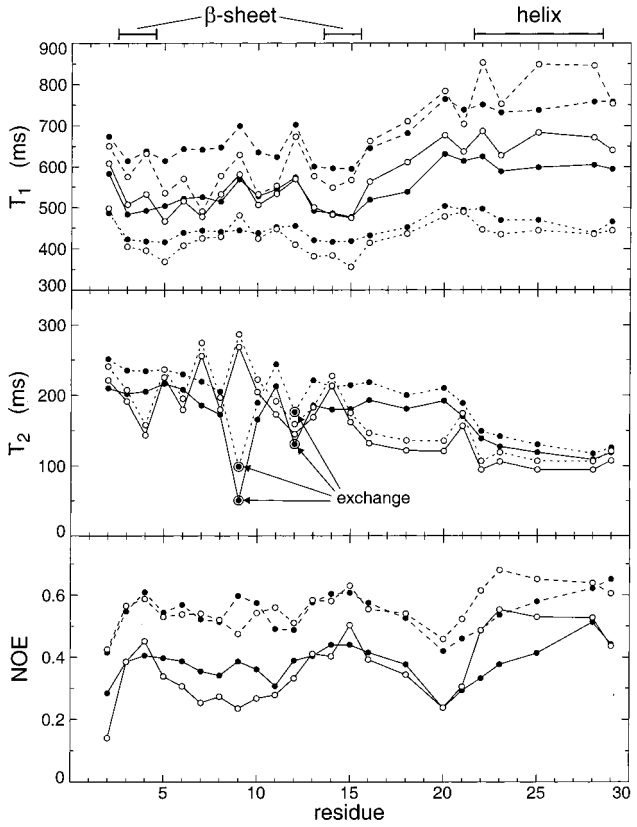

Figure 8. ^{15}N T_1 and T_2 relaxation times and {^{1}H}-^{15}N NOEs at 800 MHz (dashed line), 600 MHz (solid line), and 400 MHz (dotted line) proton frequency for the N-terminal half of the A-state of ubiquitin. Experimental relaxation parameters are shown as filled circles. Relaxation parameters calculated using the iRED analysis of rank 2 applied to the 40 ns A-state MD trajectory after fitting the correlation times of the 10 largest modes m = 18, ..., 27 are shown as open circles.

Table 2. Correlation Times for the A-State

	original MD	fitted[a]
τ_{27} (ps)	1631	9574 ± 179
τ_{26} (ps)	1132	3702 ± 190
τ_{25} (ps)	1415	2603 ± 356
τ_{24} (ps)	1565	7750 ± 295
τ_{23} (ps)	2420	9721 ± 289
τ_{22} (ps)	1185	1373 ± 56
τ_{21} (ps)	868	1360 ± 51
τ_{20} (ps)	700	24 ± 3
τ_{19} (ps)	887	1125 ± 87
τ_{18} (ps)	567	900 ± 55

[a] Standard deviations determined from a Monte Carlo error analysis consisting of 50 simulations.

largest modes $m = 18$, ..., 27 further improves the fit ($\chi^2 = 1.42 \times 10^3$). The adjusted correlation times for the 10-parameter fit are given in Table 2 together with the original values. The best fitting relaxation parameters are plotted in Figure 8.

The characteristic B_0-field dependence of the experimental data is generally well reproduced by the fit. In the experimental data, three regions with distinct relaxation behavior can be identified: the β-sheet (residues 2−15 including the loop between the two strands), the helix (residues 22−29), and a hinge region connecting the sheet and the helix (residues 16−21). These trends are well reproduced by the fitted data, except for the T_2 data of the hinge region where the fitted T_2 times have a systematic offset toward shorter values. The original estimates for the correlation times of the five largest modes are too small, while for the other five modes, the adjusted correlation times do not differ much from the original estimates, except for mode 20, which is shortened to 24 ps.

Brutscher et al.[34] analyzed ^{15}N relaxation data of the A-state on a residue-by-residue basis using an extended version of the model-free approach. This involved five independent parameters per residue including an individual overall tumbling correlation time τ_c and a fast and a slow internal correlation time associated with a fast and slow order parameter, respectively. The model-free analysis was repeated here for the N-terminal 29 residues using the same parameters for the N−H distance and ^{15}N CSA as for the iRED analysis ($r_{NH} = 1.04$ Å and $\Delta\sigma = -176$ ppm). The results of the extended model-free analysis and iRED are compared in Figure 9 for four residues at the following positions in the protein sequence: Lys 11 is located in the loop region between the two β-strands, Leu 15 is in the β-sheet, Asp 21 is in the hinge region between the sheet and the helix, and Asn 25 is in the helix. The $\delta S^2_{j,m}$ versus τ_m values obtained from the iRED analysis are superimposed on the extended model-free parameters (S^2 vs τ_c, A_1 vs τ_1, and A_2 vs τ_2) for each of the four residues, where A_k ($k = 1, 2$) are the contributions to $1 - S^2$ with correlation times τ_k. Both analyses cover a similar range of correlation times. In a few cases, such as for the slowest time-scale contributions to residue 25, a model-free data pair directly corresponds to an iRED mode contribution. In most cases, however, the model-free parameters provide a "coarse-

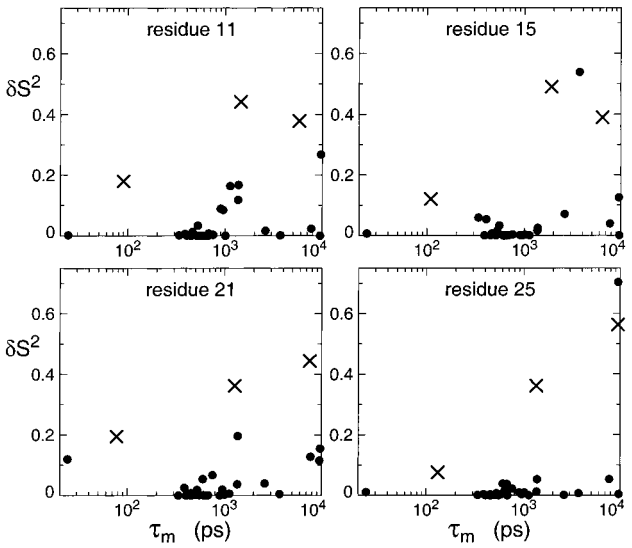

Figure 9. Eigenmode order parameter components $\delta S^2_{j,m}$ vs correlation times τ_m (filled circles) for residues Lys 11 (loop between β-strands), Leu 15 (β-sheet), Asp 21 (hinge region between the sheet and the helix), and Asn 25 (helix). τ_m was adjusted for the 10 largest modes $m = 18, ..., 27$. Also shown as crosses are the parameters from an extended model-free analysis:[34] S^2 vs τ_c, A_1 vs τ_1, and A_2 vs τ_2.

grained" representation of the more detailed iRED dynamics parameters.

6. Discussion and Conclusion

Over the past, NMR relaxation measurements of proteins have provided a wealth of spatially resolved information on motional amplitudes and time scales. Standard procedures for data interpretation including the model-free approach, analytical models, and MD-based procedures can provide insightful information for globular protein systems where internal motions can be defined with respect to a reference frame defined by the average positions of all atoms or a subset thereof. On the other hand, for highly mobile polypeptide states that do not fulfill the fundamental assumption of separability between internal and overall motions, these approaches are not applicable any longer, or the physical meaning of the fit parameters becomes unclear.

The isotropic reorientational eigenmode analysis approach introduced here addresses dynamics in the laboratory frame. Its main features are: (i) the spatial information about protein motion is described in terms of variances and covariances of the spherical harmonics representing the lattice parts of the modulated spin interactions; (ii) the isotropy of the protein ensemble is exploited, which considerably simplifies the covariance matrix and its analysis.

In principle, it is possible to construct covariance matrix **M** from relaxation experiments by measuring auto- and cross-correlated relaxation parameters at various magnetic fields to reconstruct spectral density functions and, by inverse Fourier transformation, the auto- and cross-correlation functions $C_{\mu\nu}(t)$ of all interaction pairs $\mu\nu$. Element $M_{\mu\nu}$ of matrix **M** is then directly proportional to $C_{\mu\nu}(0)$. In practice, however, cross-correlated relaxation rates of spin interactions that are far apart are difficult to measure. Therefore, an alternate route was chosen here that uses MD simulations for the evaluation of the matrix elements of **M**. Because protein MD trajectories are currently too short to produce an isotropic distribution of conformers, each snapshot is represented in the covariance matrix by an infinitely large number of isotropically reoriented replicas. The same strategy is used in the isotropically distributed ensemble (IDE) analysis method.[60]

Inspection of the eigenvalue distribution of **M** and of the separability index g_L allows one to quantitatively assess how well separability of overall and internal motions is fulfilled. In contrast, the reorientational eigenmodes of **M** reflect the correlated modulations of different spin interactions. Initial guesses for the correlation times of each reorientational eigenmode are obtained from the time-correlation functions of the projection coefficients of the snapshots on the modes.

Application of the method to backbone ^{15}N relaxation parameters of native ubiquitin yields a separability index of $g_2 = 6.3$, indicating that, as one would expect for such a globular protein system, overall and internal motions are separable in good approximation. Adjustment of only 10 correlation times belonging to the largest amplitude modes yields good agreement between theory and experiment for the 310 relaxation parameters collected for this protein. For comparison, a standard model-free analysis involves $2 \cdot 62 + 1 = 125$ fit parameters leading to a lower χ^2 value but without offering information about motional correlations between different N−H vectors. The iRED analysis of rank 2 provides such information. It decomposes S^2_j order parameters into the principal order parameter components $\delta S^2_{j,m}$, which correspond to the contribution of mode m to the modulation of spin interaction j. The $1 - S^2_j$ values are recovered by summation of $\delta S^2_{j,m}$, over the internal modes m'.

The correlation times of the five overall tumbling modes contain useful information about the rotational diffusion tensor and its anisotropy. Because these eigenmodes do not necessarily coincide with the principal axes of the diffusion frame, the correlation times yield an estimate of the lower bound of the tumbling anisotropy. Isotropic RED fundamentally differs in objective and method from the mode-coupling Smoluchowski dynamics approach.[26−29] The latter aims at a prediction of overall tumbling behavior of a fluctuating protein system using a semiempirical Smoluchowski dynamics approach.[26,29] Isotropic RED, on the other hand, is based on a principal component analysis of irreducible lattice functions. The overall tumbling observed during a finite MD trajectory is extrapolated to an isotropic ensemble, and correlation times are empirically adjusted to optimally reproduce experimental NMR relaxation parameters. Isotropic RED is also entirely different from the recently proposed structural mode-coupling approach,[62] which characterizes dynamics independently for different sites, whereas iRED represents a collective description of reorientational motions.

For a "well-behaved" globular protein that fulfills the separability condition, such as native ubiquitin, iRED is similar to the RED approach,[8] except that no decision has to be made with respect to the choice of the overall tumbling model. The particular strength of iRED becomes apparent when the separability between overall and internal motions breaks down. This situation applies for the partially folded and highly mobile

(62) Tugarinov, V.; Liang, Z.; Shapiro, Y. E.; Freed, J.; Meirovitch, E. *J. Am. Chem. Soc.* **2001**, *123*, 3055−3063.

A-state analogue of ubiquitin for which the gap in the iRED amplitude distribution between internal modes and overall tumbling modes vanishes (Figure 5), which is also accompanied by a small separability index $g_2 = 2.51$. Thus, a distinction between internal and overall modes is impossible for this partially folded state. Because during the simulation the helix remains more intact than does the sheet, which undergoes significant internal fluctuations, the 10 largest-amplitude modes of Figure 6 modulate mainly N−H vectors belonging to the sheet. The largest mode, which affects the helix as a whole together with selected N−H vectors of the sheet, and mode 23, which mainly operates on the hinge region (residues 16−21) that connects the sheet and the helix, are the exceptions.

When separability breaks down, S_j^2 order parameters of eq 6 become zero, while the mode-specific principal order parameter components $\delta S_{j,m}^2$ remain informative. Because some of the correlation times exhibited by the A-state simulation fall into the nanosecond range, the separability index decreases with increasing simulation time. For example, for the first 5 ns of the 40 ns segment, which was described previously,[44] $g_2 = 3.69$, indicating that separability is better fulfilled for this subsegment of the trajectory.

Satisfactory agreement between experiment and theory is achieved by adjusting the correlation times of some of the largest amplitude modes by up to a factor of 6 (Table 2). Thus, the iRED analysis indicates for the N-terminal half of the A-state fundamental agreement between the MD trajectory and the NMR data. The dynamics of the A-state cover a wider range of correlation times than does native ubiquitin as is already seen when triexponential correlation functions are fitted to the relaxation parameters of individual backbone ^{15}N nuclei.[34] The iRED results corroborate and refine these findings yielding an even wider distribution of time scales displayed in Figure 9. In fact, the extended model-free parameters can be viewed as a coarse-grained amplitude and correlation time distribution of the iRED distribution.

In a recent study, NMR relaxation parameters of the natively unfolded form of pro-peptide subtilisin could be interpreted using a continuous Cole−Cole distribution for slow correlation times together with a single "local" correlation time.[40] For the ubiquitin A-state, the iRED analysis also suggests the presence of multiple slow correlation times (Figure 9). A Cole−Cole-like correlation-time distribution is, however, not apparent.

In summary, the iRED method provides a general framework for the characterization of macromolecular dynamics on nano- and subnanosecond time scales. Unlike most other approaches for NMR relaxation interpretation, it is not restricted to globular systems for which overall and internal motions are well separable. The approach provides reorientational eigenmode information depicting correlated dynamics of different polypeptide parts together with mode-specific correlation times. Isotropic RED is applicable to a large variety of macromolecular systems irrespective of their shape and whether they are folded, partially folded, or unfolded, including single and multidomain proteins, peptides, nucleic acids, and polymers in solution.

Acknowledgment. J.J.P. acknowledges a long-term postdoctoral fellowship of the Human Frontier Science Program. This work was supported by NSF Grant MCB-9904875.

Appendix

A1. Spectral Densities and NMR Relaxation Parameters. The spectral density function of eq 1 enters the standard expressions for the T_1, T_2, and NOE relaxation parameters according to the relaxation theory of Bloch, Wangsness, and Redfield.[45,46] The longitudinal relaxation rate $1/T_1$ of a ^{15}N nucleus is given by

$$\frac{1}{T_{1,j}} = \frac{1}{20}\left(\frac{\mu_0}{4\pi}\right)^2\left(\frac{h}{2\pi}\right)^2 \gamma_N^2\gamma_H^2\langle r_{NH}^{-3}\rangle^2 \times \{3J_j(\omega_N) + J_j(\omega_H - \omega_N) + 6J_j(\omega_H + \omega_N)\} + \frac{1}{15}\omega_N^2(\Delta\sigma)^2 J_j(\omega_N) \quad \text{(A1)}$$

where μ_0 is the permeability of vacuum, h is Planck's constant, γ_N, γ_H are the gyromagnetic ratios of ^{15}N and ^{1}H nuclei, $\Delta\sigma$ is the chemical shielding anisotropy constant, and r_{NH} is the N−H distance. ω_N and ω_H are the Larmor frequencies (in rad/s) of the ^{15}N and ^{1}H nuclei, respectively. The corresponding expressions for $1/T_2$ and the $\{^1$H$\}$-^{15}N NOE are

$$\frac{1}{T_{2,j}} = \frac{1}{40}\left(\frac{\mu_0}{4\pi}\right)^2\left(\frac{h}{2\pi}\right)^2 \gamma_N^2\gamma_H^2\langle r_{NH}^{-3}\rangle^2 \times \{4J_j(0) + 3J_j(\omega_N) + J_j(\omega_H - \omega_N) + 6J_j(\omega_H) + 6J_j(\omega_H + \omega_N)\} + \frac{1}{90}\omega_N^2(\Delta\sigma)^2\{4J_j(0) + 3J_j(\omega_N)\} \quad \text{(A2)}$$

$$\mathrm{NOE}_j = 1 + \frac{\gamma_H}{\gamma_N} T_{1,j}\Gamma_j \quad \text{(A3)}$$

where $\Gamma_j = 1/20(\mu_0/4\pi)^2(h/2\pi)^2\gamma_N^2\gamma_H^2\langle r_{NH}^{-3}\rangle^2\{6J_j(\omega_H + \omega_N) - J_j(\omega_H - \omega_N)\}$ is the ^{1}H → ^{15}N cross-relaxation rate constant.

A2. Isotropic Average of the Covariance Matrix of Spherical Harmonics of Rank *L*. For each MD snapshot, a $n(2L + 1)$-dimensional vector $|Y(t)\rangle$ can be constructed from the spherical harmonics $Y_{LM}(\Omega_j)$ evaluated at the n directions $\Omega_j(t) = (\theta_j(t), \varphi_j(t))$, $j = 1, ..., n$, of the internuclear vectors[8]

$$|Y(t)\rangle = |Y_{L,-M}(\Omega_1), Y_{L,-M+1}(\Omega_1), ..., Y_{L,M-1}(\Omega_1), Y_{LM}(\Omega_1), ... Y_{L,-M}(\Omega_n), Y_{L,-M+1}(\Omega_n), ..., Y_{L,M-1}(\Omega_n), Y_{LM}(\Omega_n)\rangle \quad \text{(A4)}$$

The $n(2L + 1) \times n(2L + 1)$ covariance matrix $\mathbf{P}$ is then constructed as[8]

$$\mathbf{P} = \overline{(|Y\rangle - \overline{|Y\rangle})(\langle Y| - \overline{\langle Y|})} = \overline{|Y\rangle\langle Y|} - \overline{|Y\rangle}\,\overline{\langle Y|} \quad \text{(A5)}$$

where $\langle Y|$ is the complex-conjugate row vector of column vector $|Y\rangle$. The horizontal bar indicates an ensemble average over the N conformations or a time average over a trajectory.

An analytical expression is now derived for the isotropically averaged matrix $\mathbf{P}$: $\mathbf{Q} = \langle\mathbf{P}\rangle_{iso}$. The term $\overline{|Y\rangle}\,\overline{\langle Y|}$ of $\mathbf{P}$ in eq A5 averages to zero for $L \neq 0$, since $\langle Y_{LM}(\Omega)\rangle_{iso} = \int \mathrm{d}\alpha \sin\beta\, \mathrm{d}\beta\, \mathrm{d}\gamma\, Y_{LM}(\Omega) = 0$. The isotropic averaging of the term $\overline{|Y\rangle\langle Y|}$ can be carried out considering individual matrix elements $P_{M'k,M''l}$ and by using the well-known transformation properties of

spherical harmonics under 3D rotation $\mathbf{R}(\alpha, \beta, \gamma)$ defined by the three Euler angles α, β, γ:[64]

$$\mathbf{R}(\alpha, \beta, \gamma)Y_{LM}(\Omega) = \sum_{M'} D^{L}_{M'M}(\alpha, \beta, \gamma)Y_{LM'}(\Omega) \quad \text{(A6)}$$

where $D^{L}_{M'M}(\alpha,\beta,\gamma)$ are the Wigner matrix elements. It follows

$$Q_{M'k,M''l} = \langle P_{M'k,M''l}\rangle_{\text{iso}} = \overline{\langle Y_{LM'}(\Omega_k)Y_{LM''}{}^*(\Omega_l)\rangle_{\text{iso}}} = \overline{\langle \mathbf{R}(\alpha,\beta,\gamma)Y_{LM'}(\Omega_k)\mathbf{R}^{\dagger}(\alpha,\beta,\gamma)Y_{LM''}{}^*(\Omega_l)\rangle_{\alpha\beta\gamma}} \quad \text{(A7)}$$

$$= \frac{1}{8\pi^2}\sum_{N',N''}\int \mathrm{d}\alpha \sin\beta\, \mathrm{d}\beta\, \mathrm{d}\gamma \times \overline{D^{L}_{N'M'}(\alpha,\beta,\gamma)Y_{LN'}(\Omega_k)D^{L}_{N''M''}{}^*(\alpha,\beta,\gamma)Y_{LN''}{}^*(\Omega_l)} \quad \text{(A8)}$$

$$= \frac{1}{8\pi^2}\sum_{N',N''}\overline{Y_{LN'}(\Omega_k)Y_{LN''}{}^*(\Omega_l)}\frac{8\pi^2}{2L+1}\delta_{M',M''}\delta_{N',N''} \quad \text{(A9)}$$

$$= \frac{\delta_{M',M''}}{2L+1}\sum_{N'=-L}^{L}\overline{Y_{LN'}(\Omega_k)Y_{LN'}{}^*(\Omega_l)} = \frac{\delta_{M',M''}}{4\pi}\overline{P_L(\cos(\Omega_k - \Omega_l))} \quad \text{(A10)}$$

where $P_L(x)$ is the Legendre polynomial of order L, and $\Omega_k - \Omega_l$ denotes the angle between directions Ω_k and Ω_l. $\delta_{M',M''}$ denotes the Kronecker δ. Equation A9 was obtained from eq A8 by using the orthonormality relationship of Wigner matrix elements,[64]

$$\int \mathrm{d}\alpha \sin\beta\, \mathrm{d}\beta\, \mathrm{d}\gamma\, D^{L}_{M'N'}(\alpha,\beta,\gamma)D^{L}_{M''N''}{}^*(\alpha,\beta,\gamma) = \frac{8\pi^2}{2L+1}\delta_{M'M''}\delta_{N'N''} \quad \text{(A11)}$$

and eq A10 was obtained from eq A9 by using the addition theorem of spherical harmonics[64]

$$P_L(\cos(\Omega_k - \Omega_l)) = \frac{4\pi}{2L+1}\sum_{N'=-L}^{L}Y_{LN'}(\Omega_k)Y_{LN'}{}^*(\Omega_l) \quad \text{(A12)}$$

A number of features are worth mentioning:

(1) Because of isotropic averaging, the elements of matrix **Q** depend only on intramolecular angles, $\Omega_k - \Omega_l$, and not on the overall orientation any longer.

(2) Matrix **Q** can be represented as the direct matrix product

$$\mathbf{Q} = \frac{1}{4\pi}\mathbf{M}\otimes\mathbf{1} \quad \text{(A13)}$$

where **1** is a $2L + 1$-dimensional unity matrix, and **M** is a $n \times n$ matrix with elements

$$M_{kl} = \overline{P_L(\cos(\Omega_k - \Omega_l))} \quad \text{(A14)}$$

Each eigenvalue of **Q** is (at least) $2L + 1$ times degenerate, and all information contained in **Q** is also contained in **M**. Thus, the spherical symmetry introduced by isotropic averaging leads to a substantial simplification of the covariance matrix **Q**.

(3) Matrixes **Q** and **M** can be diagonalized, $\mathbf{Q}|q\rangle = \lambda_q|q\rangle$ and $\mathbf{M}|m\rangle = \lambda_m|m\rangle$, where the eigenvectors of **Q** can be easily constructed from the eigenvectors of **M**:

$$|q\rangle = |m\rangle \otimes |e_j\rangle \quad \text{(A15)}$$

where $|e_j\rangle$ are the $2L + 1$-dimensional column vectors $|e_1\rangle = (1, 0, ..., 0)^T$, $|e_2\rangle = (0, 1, ..., 0)^T$, ..., $|e_{2L+1}\rangle = (0, 0, ..., 1)^T$.

(4) The diagonal elements of **Q** are $Q_{ii} = 1/(4\pi)$, and the diagonal elements of **M** are $M_{ii} = 1$. The traces of **Q** and **M**, which are the sum of their respective eigenvalues (mode amplitudes), are proportional to the number of vectors n:

$$Tr\{\mathbf{Q}\} = n(2L + 1)/(4\pi), \quad Tr\{\mathbf{M}\} = n \quad \text{(A16)}$$

A3. Correlation Times of Individual Modes. In matrices **Q** and **M**, the time-sequence information of the snapshots is lost. Therefore, motional correlation times associated with individual reorientational eigenmodes cannot be determined from **Q** and **M**. Correlation functions can be reconstructed by projecting vector $|Y(t)\rangle$ of eq A4 constructed from the snapshot at time t on eigenvector $|q\rangle$, $a_q(t) = \langle q|Y(t)\rangle$, which leads to the correlation function

$$C_q(t) = C_{m,l}(t) = \langle a_{m,l}{}^*(\tau + t)\cdot a_{m,l}(\tau)\rangle_\tau \quad \text{(A17)}$$

where $q = (2L + 1)m + l - L$, and $l = -L, ..., L$. The average extends over snapshots sampled at times $\tau = 0 \rightarrow T - t$.

Correlation functions for **M** are obtained by summing up the $2L + 1$ correlation functions $C_{m,l}(t)$

$$C_m(t) = \sum_{l=-L}^{L}C_{m,l}(t) \quad \text{(A18)}$$

that belong to the $2L + 1$ degenerate modes q. If the correlation function $C_m(t)$ decays exponentially, the correlation time τ_m associated with mode $|m\rangle$ is determined by[9]

$$\tau_m \cong \frac{1}{C_m(0) - C_m(t \rightarrow T)}\int_0^T (C_m(t) - C_m(t \rightarrow T))\, \mathrm{d}t \quad \text{(A19)}$$

where $C_m(t \rightarrow T)$ symbolizes the plateau value of $C_m(t)$:

$$C_m(t \rightarrow T) = \sum_{l=-L}^{L}C_{m,l}(t \rightarrow T) \cong \sum_{l=-L}^{L}|\langle a_{m,l}(\tau)\rangle_\tau|^2 \quad \text{(A20)}$$

For systems where internal and overall tumbling motions are *separable*, $C_{m,l}(t)$ and $C_m(t)$ and their correlation times reflect both internal motions and overall motions. It is shown in the Supporting Information that for isotropic tumbling with correlation time τ_c, the *effective* correlation time τ_m of an *internal* mode with an internal correlation time τ_m' is given by

$$1/\tau_m = 1/\tau_c + 1/\tau_m' \quad \text{(A21)}$$

which is analogous to the situation encountered in analytical motional models and in the model-free approach.

A4. Time-Correlation Functions for Individual Interactions. We consider the case $L = 2$. The contribution of

(63) Koradi, R.; Billeter, M.; Wüthrich, K. *J. Mol. Graphics* **1996**, *14*, 29−32.
(64) Zare, R. N. *Angular Momentum*; John Wiley & Sons: New York, 1988.

mode m to the decay of the correlation function of interaction j of eq 2 is the principal order parameter component

$$\delta S^2_{j,m} = \lambda_m(|m\rangle\langle m|)_{jj} \tag{A22}$$

where $\delta S^2_{j,m} \geq 0$, and $\sum_m \delta S^2_{j,m} = 1$. The correlation function $C_j(t)$ can be expressed as a weighted sum of the normalized correlation functions $C_m(t)$, that is, $C_m(0) = 1$, belonging to iRED modes m

$$C_j(t) = \sum_m \delta S^2_{j,m} C_m(t) \tag{A23}$$

where m numbers all reorientational eigenmodes, including overall and internal motions, leading to a complete decorrelation at long times $C_j(t \rightarrow \infty) = 0$. If $C_m(t)$ is monoexponential, $C_m(t) = e^{-t/\tau_m}$, as was found to be the case in good approximation for nearly all modes, the real part of spectral density function $J_j(\omega)$ of eq 1 is obtained by analytical cosine-transformation

$$J_j(\omega) = \int_{-\infty}^{\infty} C_j(t) \cos \omega t \, dt = \sum_m \delta S^2_{j,m} \frac{2\tau_m}{1 + \omega^2 \tau_m{}^2} \tag{A24}$$

Equation A24 provides a formulation of the spectral density function in terms of principal order parameter components $\delta S^2_{j,m}$ of the covariance matrix **M** and the correlation times τ_m. The τ_m parameters can be used as fitting parameters as discussed in the text.

A5. Eigenmode Collectivity κ. A measure for the degree of collectivity of an eigenmode is the number of vectors that are significantly affected by this mode. A suitable measure is the collectivity κ[65]

$$\kappa_m = \frac{1}{n} \exp\{-\sum_{k=1}^{n} \left|\,|m\rangle_k\right|^2 \log\left|\,|m\rangle_k\right|^2\} \tag{A25}$$

where $|m\rangle_k$ is the kth component of the normalized eigenvector $|m\rangle$. κ ranges between $1/N$ and 1 and gives the fraction of vectors expressed as the total percentage that is significantly affected by reorientational eigenmode $|m\rangle$.

A6. Separability Measure. A measure for the separability of overall and internal motions is defined by the separability index[60]

$$g_L = \sum_{i=1}^{n} \lambda_i \Big/ \sum_{i=1}^{n-(2L+1)} \lambda_i \tag{A26}$$

where the eigenvalues λ_i of the covariance matrix are sorted with respect to their magnitude. The numerator corresponds to the trace of the covariance matrix ($=n$), while the denominator corresponds to the trace minus the $2L + 1$ largest eigenvalues. The larger the g_L, the better separable are the overall and internal motions. In the limiting case of a static structure, $g_L \rightarrow \infty$.

Supporting Information Available: Figures with distributions of iRED correlation times of native ubiquitin and the A-state. Theoretical treatment of the effect of overall tumbling motion on correlation times of internal iRED modes (PDF). This material is available free of charge via the Internet at http://pubs.acs.org.

JA012750U

(65) Prompers, J. J.; Lienin, S. F.; Brüschweiler, R. In *Biocomputing: Proceedings of the 2001 Pacific Symposium*; Altman, R. B., Dunker, A. K., Hunter, L., Lauderdale, K., Klein, T. E., Eds.; World Scientific: Singapore, 2001; pp 79−88.